3D Printed Kerf Structures

Osazuwa John Okundaye-Santos Jr
Architecture
Texas A&M University
College Station, Texas, United States
awuzaso@tamu.edu

Kamal poluri
Mechanical Engineering
Texas A&M University
College Station, Texas, United States
kamalp@tamu.edu

Aryabhat Darnal
Mechanical Engineering
Texas A&M University
College Station, Texas, United States
adarnal@tamu.edu

Anastasia Hanifah Muliana
Texas A&M University
College Station, Texas, United States
amuliana@tamu.edu

Jeeeun Kim
Computer Science & Engineering
Texas A&M University
College Station, Texas, United States
jeeeun.kim@tamu.edu

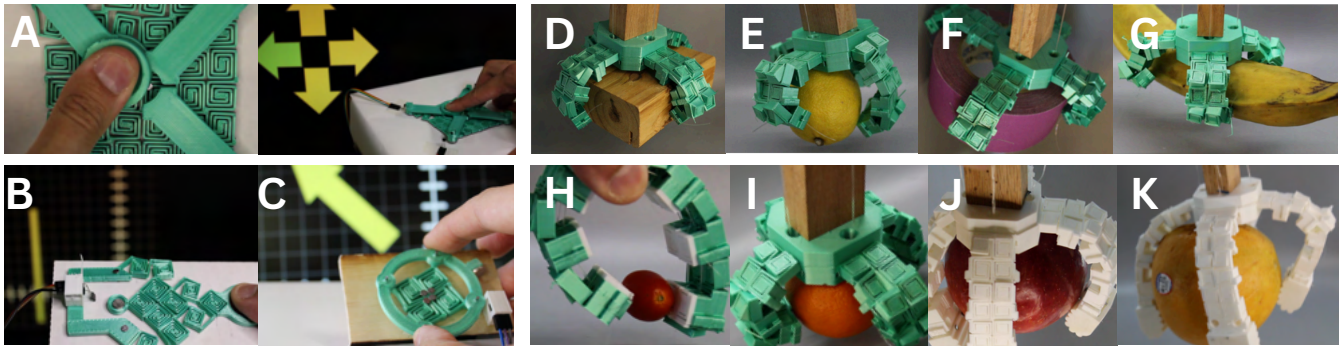

Figure 1: 3D printed kerf structures support various interaction affordances, a slider controller (A), a pinball-type spring input device (B), a rotational dial (C), a four-finger gripper that handles objects of different shapes, sizes, textures, and weights (D–G). Modifying various geometry and material parameters, the gripper modifications become a two-finger gripper with a TPU top layer, for small cherry tomatoes to tangerines to slippery apples to large, heavy grapefruits using TPU-based claws (H–K).

Abstract

Kerfing is a well-known method in subtractive manufacturing used to create flexible surfaces from stiff planar materials. In this work, we study 3D-printed kerfing to enable freeform movement in rigid polymer materials suitable for FDM (Fused Deposition Modeling). Designers and end users can leverage kerf structures due to their ability to bend in single, double, or multiple axes. With the accessibility of consumer-grade 3D printers, kerf structures offer an easy approach to fabricating freeform structures and compliant mechanisms for interactive primitives and applications like grippers.

Building on the principles and mechanics of traditional subtractive kerf structures, we propose that 3D-printed kerf structures can be modified by varying the shape, cell density, and alignment of cells, which influence their deformation and load-bearing capabilities. Additionally, we examine how the unique advantages of 3D printing can further augment the capabilities of kerfing, such as through multi-material printing (e.g., applying a thin TPU layer over PLA at contact points of a kerf-structured gripper for improved friction) or bilayer structures (e.g., using a one-to-one proportion of PLA and TPU material overlaid over one another in the kerf structure for a wearable sensor band). We validate our approach through various applications and the interaction spaces created by kerf designs, such as tangible user interfaces with tunable haptic feedback and robotic grippers.

CCS Concepts

• **Human-centered computing** → **Interaction devices**.

Keywords

Tangible user interface; 3D printing

ACM Reference Format:
Osazuwa John Okundaye-Santos Jr, Kamal poluri, Aryabhat Darnal, Anastasia Hanifah Muliana, and Jeeeun Kim. 2025. 3D Printed Kerf Structures. In *Nineteenth International Conference on Tangible, Embedded, and Embodied Interaction (TEI '25), March 04–07, 2025, Bordeaux / Talence, France.* ACM, New York, NY, USA, 15 pages. https://doi.org/10.1145/3689050.3704941

TEI '25, March 04–07, 2025, Bordeaux / Talence, France

ACM ISBN 979-8-4007-1197-8/25/03
https://doi.org/10.1145/3689050.3704941

1 Introduction

Kerf structures are created through subtractive fabrication from stiff planar materials, such as sheets of plywood, medium-density fiberboard (MDF), and metal (Figure 2) [10]. Similar to kirigami [3, 34], flexibility in stiff objects is achieved by making slender cut patterns, strategically removing portions to make rigid materials more flexible. This method can turn even a thick, stiff plywood panel into a flexible 3D form. By allowing deformation in multiple directions [8, 24, 42], rigid materials can bend over a length and act as their own hinge, similar to living hinges [25]. Spatial factors of kerf topology, including density, cell size, and beam thickness, can control the local mechanical properties of the structure. Through this approach, kerfing imparts flexibility in rigid objects while minimizing stresses in its deformation [10, 36].

Figure 2: Kerf structures are often the results of subtractive fabrication, imparting flexibility to rigid sheets.

While kerfing effects originate from subtractive manufacturing processes, they can also be replicated in additive manufacturing. With the increasing accessibility of 3D printing, creating complex surfaces that bend in single, double, or multiple axes using kerfing [25, 36] becomes feasible and more accessible to a wider audience (Figure 3 A). We demonstrate that 3D printed kerf structures can be deformed by opposing in-plane forces (Figure 3 B) and out-of-plane by way of folding (Figure 3 C) and twisting (Figure 3 D). This enables designers and users to create flexible objects and devices with minimal assembly or post-production. Kerfing effects can be applied to additive manufacturing by defining 3D object geometry through kerf-cut patterns on the intended thickness. Kerfing effects, driven by the dynamics of cut and uncut portions rather than the manufacturing method [4, 41], have implications for mechanical and interactive affordances towards the HCI research community:

(1) Applying kerfing to 3D printed objects can enhance their structural flexibility.
(2) Understanding the interplay between kerfing behaviors (geometry) and material responses (materials) in 3D printing enables coupling of kerfing behaviors with other 3D printing exclusive printing factors (e.g., bi-layer composition or techniques for 4D printing) so to program the extent of flexibility and durability of interactive objects.
(3) By understanding how kerf patterns are implemented in subtractive manufacturing, designers can transpose kerf geometric properties to additive manufacturing to create interactive 3D printed objects.

We argue that 3D printing can be used as an alternative method for imparting freeform movement to rigid flat base materials. 3D printing leverages principles of subtractive kerf structures to create 3D forms with dynamic microstructural behaviors by adjusting cell density and printed geometry alignment [19]. 3D printing offers advantages in fabricating kerf structures, such as using materials like PLA or TPU for varying deformation and combining materials (e.g., PLA and TPU in bi-layer compositions [11]) or programmable filaments [27] for specific behaviors. This can benefit designers in fabricating interactive applications, such as tangible user interfaces with tunable haptic feedback and robotic grippers (Figure 1).

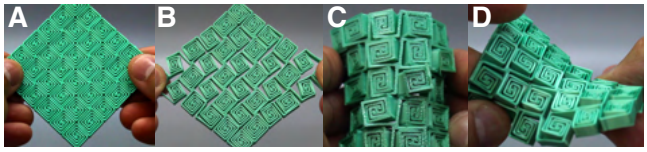

Figure 3: 3D-Printed Kerf structures (A) embrace all mechanical traits of 2D-Laser cut structures, with the additional benefit of integrating various material-oriented benefits, presenting wider interaction affordance, pulling (B), bending/folding (C), and twisting (D).

To explore how 3D-printed kerf structures support interactive object design, we examine their mechanical functions and potential for sensing and haptic applications. This paper addresses the following research questions:

- **RQ 1:** How can varying the microstructure of kerf-patterns influence deformation output towards sensing/haptic applications towards interactive devices?
- **RQ 2:** What are the advantages of employing multi-material fabrication in the design of 3D kerf structures?

Seeking answers resulted in our contribution as follows:

- Characterization of 3D printed kerf design and how their mechanical responses relate to specific deformation outcomes.
- Design guidelines of 3D printed kerf that links user input actions to output deformation behavior.
- A number of interactive device applications applying kerf deformation behaviors that can inform the mechanical considerations for interactive device design for sensing/haptic applications.

This work extends established knowledge of 2D kerf structures to 3D printing, showcasing their viability. 3D printing allows to accommodate diverse materials and geometries, more importantly, their interplays, including bi-layer and composite materials that are not a part of design space in laser cutting. The material-geometry interplay enables novel control of flexibility and reconfigurability. While traditional kerfing studies focus on geometry, we demonstrate that material behavior significantly influences deformation. To highlight this, we explore multi-material kerf structures using Fused Deposition Modeling (FDM) 3D printing for accessibility.

2 Kerfing Attributes and Fabrication Considerations: Prior Works

2.1 Interactive Devices by Metamaterials

Metamaterials are artificial structures with mechanical properties defined by repetitive microstructures (cells) rather than the material itself [33]. One such property is auxetic behavior, where a material expands laterally when stretched, becoming wider or thicker.

The deformation direction depends on the scale, orientation, and arrangement of these geometrically organized cells [19, 35]. In 3D printing, metamaterials are formed by tiled microstructures optimized into 2D or 3D lattice structures [1, 31, 35] (Figure 4 A). These lattices enable deformation either in-plane (e.g., bending soles of shoes [1]) or out-of-plane (e.g., jointed figurines [35]).

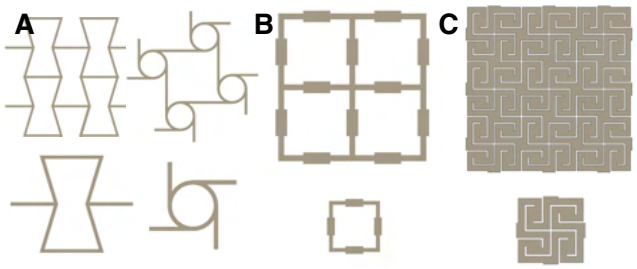

Figure 4: Lattice and hierarchical structures (A). Metamaterial mechanism shear cells (B). Square-locked kerf structure (C).

Another approach uses shear-cells, where small-scale members function as living hinges. When a force is applied, these hinges bend (Figure 4 B). Variations of shear-cells have been used to implement a number of interactive objects such as pliers, door latches, digital locks [21], tunable textures [20], and reconfigurable elasticity in items like shoes or piano keys [40].

While kerf-unit cells (Figure 4 C) resemble typical metamaterial structures (A and B), Shahid et al. highlight the unique deformation behaviors of kerf-unit cells [37]. They explain that each kerf cell is a continuous flow of slender beams folding into repeating patterns. This structure allows kerf cells to exhibit flexibility and multiple deformations through bending, twisting, and elongation/contraction. Unlike typical metamaterials, which consist of closed individual cells or progressively smaller embedded cells, kerf structures support both in-plane and out-of-plane deformations, enabling macroscopic (surface-level) and microscopic (unit-cell level) changes.

2.2 Mechanics of Kerfing

From an end-user perspective, kerfing enables the creation of flexible objects from rigid materials like wood or metal. As material is removed, rigid areas that would typically fail under force instead deform. With more cuts, the object gains flexibility across different directions and planes [41, 42]. Kerfing also alters the mechanical properties of the material, reducing the local second and polar moments of uncut areas [4, 10, 25]. These changes impact load-bearing capacity and elasticity, with the uncut sections acquiring elastic properties, allowing them to return to their original shape once the applied force is removed [10, 24]. By combining flexibility (bending without breaking) and elasticity (returning to the original shape after deformation), kerfed structures can deform and recover their default form [4, 5, 10, 24, 26]. In-plane and out-of-plane deformations in kerf-patterned objects result from the geometric dynamics between constrained points and applied forces. The organization of kerf-unit cells, both within (sub-cells) and their interconnected aggregations (compound cells), influences these deformations.

2.3 Toward 3D Printed Kerf structures

Kerf structures are typically fabricated through laser-cut fabrication processes, however, these approaches have limitations in their end-use. First, a key limitation of laser cutting is the inability to control cut gaps within different machines, as in plasma and water jet [14, 29, 38]. Second, laser cutting thicker panels can result in trapezoidal cuts, where the bottom is wider than the top (an issue typically encountered in wood kerfing) [7, 15].

3D printing kerf structures ensures precise gaps within and between layers, with one approach treating kerf geometry as a developable sheet. One common application in 3D printing is fabrication of fabrics for structural use or to enhance existing ones, for example, flexible meshes for medical implants [32] and textiles resembling weft knits [28]. Such an approach can be extended to the fabrication of planar (2D) kerf structures. Additionally, 3D printing introduces materials that enhance the deformation capabilities of kerf structures. PLA allows for tuning strength and rigidity [9, 23, 30], while TPU offers compliance adjustments and low elastic modulus, ideal for squash and stretch behaviors [9, 17]. Beyond individual filaments, multi-material printing, using bi-layer composition [11] or programmable filaments [12, 13, 27], allows for combining filament strengths to engineer material properties for improved mechanical performance [12, 13, 16, 22, 30, 39].

In 3D printing kerf structures, there are limitations in fabrication and end-use context. First, 3D printing methods like FDM produce parts with anisotropic mechanical properties, where strength and stiffness vary based on print direction [2]. Since FDM builds objects layer by layer, the bonding between layers is weaker, making them more prone to failure under load or repeated stress. In contrast, laser cutting uses materials that are typically homogeneous in two dimensions, avoiding this issue. Second, 3D printing is more resource-intensive than laser cutting. The FDM process requires time for detail and size, with constant heating and cooling cycles that consume more energy per unit of material compared to laser cutting for similar objects [2, 18].

3D-printed kerf structures offer several benefits in the fabrication of everyday interactive objects. To fully understand these advantages, we must compare 3D printing with purchasing commercially available equivalents. We argue that 3D-printed kerf structures provide: 1) more customization options, 2) greater user involvement in creation, and 3) broad applicability across various fields. We highlight these benefits by comparing our approach with examples from prior research, such as Metamaterial Mechanisms [19] and Reprise [6], as well as commercial products (Figure 5).

While commercially available products (e.g., door knobs or grippers), can be purchased and installed, 3D-printed alternatives offer distinct advantages. These devices, such as those in [6] and [19], can be customized to fit the user's context (e.g., a doorknob or extension tailored to hand dimensions). Additionally, these objects can be fabricated simply, with the mechanism printed as a single structure or with minimal sub-assemblies. Metamaterial Mechanisms [19] differ from Reprise [6] in that their mechanical design is integrated within the supporting lattice, requiring no post-assembly.

In terms of maintenance, commercially purchased objects, like a gripper, require tools, knowledge, and materials for repairs. In contrast, 3D-printed devices can be easily replaced or repaired

	Commercial Products*	Reprise [6]	Metamaterial Mechanisms [19]	3D Printed Kerf
Device Target Variability	X			X
Customizability		X	X	X
Ease of Fabrication		X	X	X
No assembly needed			X	X
Easy maintenance		X	X	X
Diversity of Materials		X	X	X
Multimaterial Affordances				X
*Examples include robotic grippers				

Figure 5: Comparison of 3D printed related features of prior work in comparison to 3D printed kerfs.

with existing parts, without specialized components or advanced reassembly skills. Another advantage of 3D-printed objects is material choice, allowing for the creation of interactive items with specific properties that enhance mechanical function. 3D-printed kerf structures combine the benefits of these approaches and enable tailored interactive outcomes by organizing geometry with different materials, such as a TPU-lined PLA gripper for better handling of textured objects. We explore how 3D-printed kerf-cells can support compliant mechanisms and how their unique capabilities can enhance these structures. Specifically, we investigate how mechanical properties are influenced by material choice and bi-layer compositions, such as combining TPU with PLA in kerf structures.

3 Anatomy of 3D Printed Kerf Structures

Kerf behaviors refer to how the organization of cut patterns—such as shape, grouping, and density—affects the flexibility and elasticity of stiff planar objects. This section outlines the components of our 3D-printable kerf-structure design, explaining how applied forces and constraints trigger deformations. We will also provide example applications for designing these deformations.

3.1 Dynamics Principle of Kerf Unit Cell Pattern Organization

Previous research has explored how variables like cut pattern shape and length affect the flexibility and elasticity of rigid objects. These studies have led to the development of several reliable kerf cut patterns, commonly used by architects and designers, that produce consistent deformation effects.

One common kerf pattern is straight-line kerfing, used for structures requiring bending in a single direction (e.g., for creating a chair's bent panel). Another is the 2D meandering spiral [24], where cuts form a series of spirals that vary in distance between successive turns. This pattern is unique because its length and increasing spiral turns reduce the force needed to deform the object, while the elastic potential energy increases linearly with the length of the spiral. A notable example of this is the 2D meandering pattern developed by Dujam Ivanisevic [41, 42], which utilizes multi-axial deformations to introduce double curvature through cut and uncut regions of rigid objects.

Due to the 2D meandering pattern's ability to support multi-axial deformation, it was studied to explore the relationship between its design variables and deformation capability. Key variables identified include shapes (e.g., square-interlocked Archimedean, triangular, and hexagonal spirals) [36, 37], levels of organization (e.g., kerf patterns as unit cells or aggregates) [5], and cut densities [36, 37].

In the following sections, we will expand on existing knowledge of digital fabrication of kerf-cut patterns, focusing on their anatomy. By examining kerf-cut patterns at various levels of organization, we will show how specific in- and out-of-plane deformations emerge from particular combinations of applied forces and constraints.

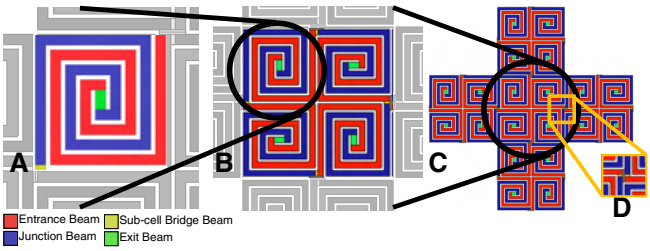

Figure 6: Sub-cellular organization of a kerf unit-cell (A), integrated into interlinked sub-cells forming a kerf unit-cell (B), presenting unique deformation behaviors in a resulting device, such as a gripper leg (C). Each exit beam of a sub-cell transitions into the next adjoining sub-cell, while neighboring unit-cells are connected by their inter-cellular beams, forming a bridge (D).

3.2 Sub-cell

Kerf sub-cells consist of sequential beams that connect and follow a spiral path (Figure 6 A). The first beam, called the entrance beam, starts from the outside of the sub-cell and spirals clockwise with a specific angular bend (90 degrees for the square-locked Archimedean kerf unit-cell pattern) at each turn. The entrance beam closes toward the center, transitions into the junction beam, and connects to the exit beam. The exit beam, defined similarly to the entrance beam, spirals counterclockwise toward the outside. Sub-cells connect by linking one sub-cell's exit beam to a contiguous sub-cell's entrance beam (Figure 6 B). The angular bend of the entrance and exit beams determines the overall shape and maximum number of cells that can be linked, defining the density of subsequent structures. Once all sub-cells are linked, they form a circuit path. Together, the linked sub-cells form a single cell. We refer to these linked sub-cells as a unit cell, which will be detailed in the following section.

Deformation of sub-cells is achieved by constraining the intercellular beams (Figure 6 D) of the kerf unit-cell and applying force to any of the junction beams. Alternatively, solid parts can be added and constrained to the junction to transmit force (Figure 7 A and B). In-plane deformation (Figure 7 C and D), while also involving constraints, occurs by pulling or pushing the geometry of its entrance beam, causing the interconnected beams to deform as the exit beam resists the force.

3.3 Unit-cell

The shape and paths of one sub-cell influence how many sub-cells can be adjoined to form a unit cell (Figure 6 B). Each exit beam

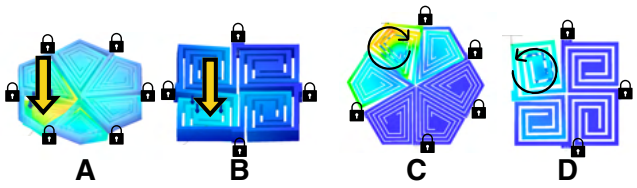

Figure 7: Sub-cell deformation of Kerf cells. Out-of-plane push deformation (A-B), and in-plane sub-cell rotational deformation (C-D) for hexagon and square kerf patterns, under 20N of force applied.

within the sub-cell acts as an entrance for the next adjoining sub-cell, continuing until there a circuit of sub-cells is formed, creating the unit-cell. The extent to which the unit cell can be deformed in-plane and out-of-plane is determined by the angle of its interconnected sub-cells' beam spirals.

Deformations are achieved by applying forces either to the junction beam (for out-of-plane deformation) or to the entrance beam (for in-plane deformation) (Figure 8). Intercellular beams serve as constraints for unit cells in the same way they do for sub-cells. Out-of-plane deformation arises from the collective force applied to the unit cell. In Figure 8 (A and B), we illustrate how this behavior results in deformation when a force is applied towards the middle of the unit cells. Due to the slender beam structure of the unit cells, most of the deformation is concentrated in the innermost beams, with the effects diminishing as the slender beam geometry transitions towards the junction beam. For in-plane deformations (Figure 8, C and D), a constraint is applied by holding the innermost beams towards the center of the unit cell in place. Force is then applied to the entrance beams in the direction opposite to the spiralized beams. This can be achieved by collectively moving the entrance beams or the junction beams in unison.

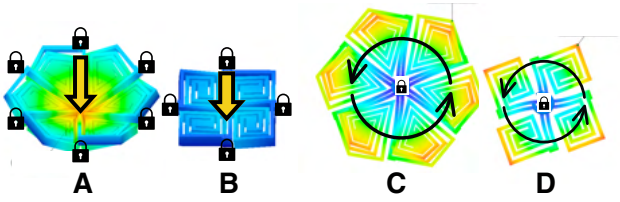

Figure 8: Unit-cell deformations with a 20 N force applied. Out-of-plane push deformation at scale of the unit-cell (A-B), and in-plane rotation kerf cell (C-D) for both hexagon and square kerf patterns.

3.4 Compound-cell

When unit cells are linked via their intercellular bridge beams, they form a compound cell as in Figure 6 (C). At least one central unit-cell is attached to other unit-cells, serving as a hub for paths entering and exiting adjoining unit-cells. Compound cells can be connected to other compound cells, creating aggregates that can be infinitely combined to form larger, complex organizations, depending on the application context.

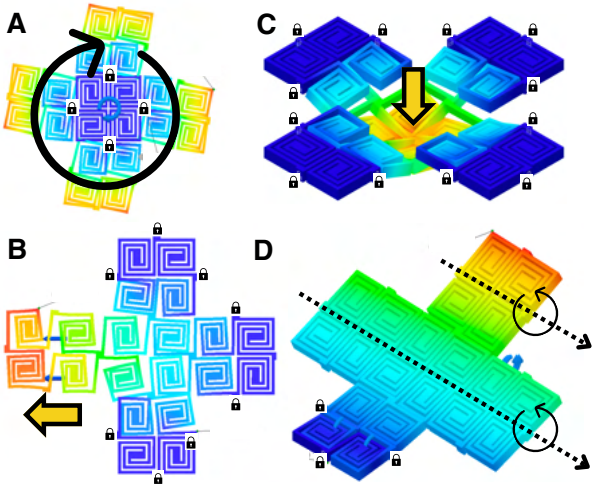

Figure 9: Compound cell deformations. (A) in-plane rotational deformation (B) out-of-plane push deformation (C) Compound in-In-plane pull deformation by single kerf-unit cell. (D) out-of-plane compound-cell rotational deformation, curling about axis where cuts locate.

Figure 9 (A) demonstrates the in-plane rotation of compound cells consisting of square sub-cells. Similar to its unit-cell equivalent, the constraint is applied towards the center of the unit cell. However, the entire unit cell can serve as a constraint, with the junction beams resisting movement, while input motion is applied to the unit cells attached to the central unit cell, and force is applied to each unit cell's entrance beams. Figure 9 (B) shows in-plane pulling as a deformation, with the constraint provided by interconnected unit cells. In the illustration, a single unit cell is pulled from the central unit cell while the others are constrained. As the left-most unit cell is pulled away, the central unit cell's left-most geometry is also pulled but restricted by the connected unit cells, resulting in a gradation of deformation effects.

Figure 9 (C) demonstrates out-of-plane behavior with a push input force applied towards the center-most unit cell, with the outer unit cells constrained by their intercellular beams. Similar to pull deformation, the deformation effects decrease gradually as the center-most unit cell's beams (exit beams) transition to the entrance beams of the outermost unit cells. Figure 9 (D) shows out-of-plane rotation in the form of curled unit-cells. In the image, a single unit cell is constrained by its intercellular beams. The remaining unit cells rotate about the central cut of connected unit-cells, starting with the constrained unit-cell. For each cut axis that is bending, the effects are shared among unit-cells that reside on that axis. We see this bending within the constrained unit-cell, the three interconnected unit-cells in the middle of the compound cell, and the furthermost unit-cell as well.

3.5 Creating Interaction Affordances: Through Applications

Kerf structures can be used as a part of tangible interactive devices; this is made possible by how they can be applied as an action layer for their output movement. This section describes ad-hoc design parameters that create visible affordances for designers and users utilizing deformation behaviors of kerf structures, presented through practical application examples.

While there are numerous kerf cut patterns and variations identified within the literature [25, 41, 42] and of the potential to explore meso and macro-scale effects, to have a tractable exploration space, we limit our exploration to better understand the core behavior of the kerf patterns. We focus on two key parameters of kerf cut designs (seen in Table 1 under section, *"Kerf Cut Pattern Parameter"*).

First, we focus on *"Kerf Pattern"*, which controls how the cut-lines are spiraled within the unit-cell shape. For this work, we examined the square-locked and hexagonal Archimedean spirals. The second kerf pattern parameter we consider is *"Cut Density"*, referring to the number of cut-line layers within the unit cell, as seen by the space between walls in the kerf-patterns, referred to as gap-width as seen in Table 1, under the *"Geometrical Properties"* section. We identify the different number of cut-line layers in terms of their relative cut density, these being low density (LD), medium density (MD), and high density (HD). LD kerf cells have the lowest number of cut lines whereas HD kerf cells have the higher number of cut lines with respect to their given pattern type.

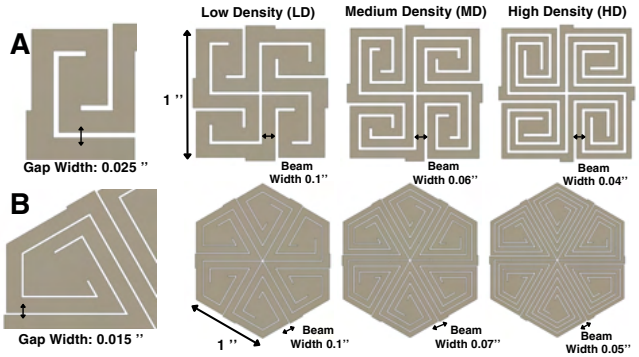

Figure 10: Visual variants of square kerf-cut pattern (A Row), and hexagon kerf-cut pattern (B Row).

The combination of the kerf-cut pattern and cut-density influences its geometrical properties (seen in Table 1), areas and gap width. The area for each kerf-pattern, (seen in column 3 of Table 1) comes from its thickness (t) and the width of its pattern variation (w). In the interest of comparison within each pattern type, the gap width (seen in column 4 of Table 1) is held constant (i.e., 0.025 and 0.015 inches for square and hexagon kerf patterns respectively) alongside side length (i.e., 1 inch for all patterns and variations) while cut lines are varied across the LD, MD, and HD kerf patterns (Figure 10 and Table 1). Table 2 summarizes the printing parameters we used in 3D printing these examples, using a Bambu P1S 3D printer alongside PLA from Bambu and TPU from OVERTURE 3D.

Kerf Cut Pattern Parameter		Geometrical Properties	
Kerf Pattern	**Cut Density**	**Beam Area (in^2) t x w**	**Gap Width (in)**
Square-Locked	LD	0.125 x 0.10	0.025
	MD	0.125 x 0.06	0.025
	HD	0.125 x 0.04	0.025
Hexagon	LD	0.125 x 0.10	0.015
	MD	0.125 x 0.07	0.015
	HD	0.125 x 0.05	0.015

Table 1: Kerf pattern parameters and geometrical Properties.

Printing Settings	PLA	TPU
Print Temperature (℃)	220	240
Print Speed (mm/s)	200	200
Infill Density (%)	15%	15%
Flowrate (%)	98%	100%
Layer Height (mm)	0.28	0.28
Raster Angle	45°	45°

Table 2: 3D printing settings for fabricating Kerf structures.

3.5.1 Attachment Handles to Guide User Input. Deforming kerf cells at any level of organization depends on where an applied force is set and where exactly its cells are constrained. Defining these two factors enables designing a handle to guide users to manipulate it. For each application in this section we will describe how its handle is designed to create a *point of force contact* and a *constraint to work against.*

Pinball Spring: One example of how handles can guide user input is our pinball spring hammer mechanism (Figure 11). The design uses square-kerf unit-cells connected as a compound unit. Pulling the corner of the rightmost cell causes it to snap back, moving a neodymium magnet to a paired Hall effect sensor. This kerf mechanism acts as an interactive controller, recording changes in the magnetic field as the cells deform. Figure 11 shows how pulling and twisting are sensed by measuring force displacements.

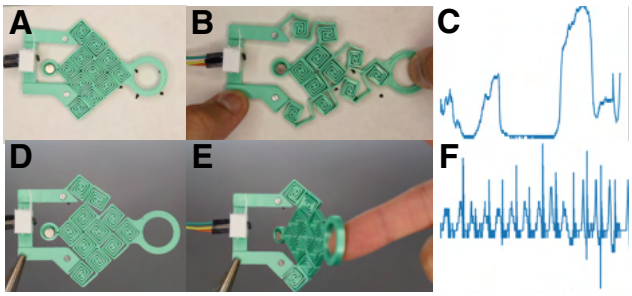

Figure 11: Square-locked kerf pattern is deformed in-plane (A-B) and sensed signals (C), and out-of-plane (D-E) creating unique signal (F) enabling sensing.

Push Button: Push buttons directly apply out-of-plane deformations through two design components. A push-button cased based on the hexagonal kerf cell (Figure 12 A) has notches for press-fit attachment of DuPont connectors with a Hall effect sensor, with the press-fit spaces located near the attached kerf unit-cell pattern piece (B–D). The user applies force to the raised section of the kerf pattern to cause deformation, sensed through displacement between 2.5*mm* magnet and hall effect sensor. The modular design allows users to switch among hexagon kerf pattern variations to control the extent and speed of deformation. The high-density cut pattern (Figure 12 B), with a high-density (HD) cut, offers softer, spring-like haptic feedback, while low density (LD) cut pattern (C) , is slower and requires more force to achieve the same deformation depth. The medium density cut, a medium cut density (MD) pattern, falls between the high and low cut density patterns in terms of haptic feedback and force required to push.

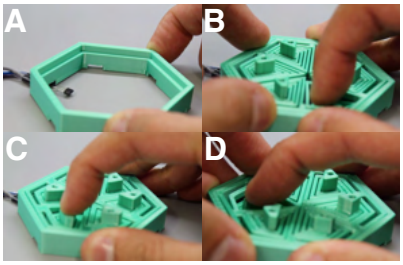

Figure 12: Push buttons use sub-cell deformations for interaction. (A) Case holds hexagon kerf cell (with magnet) and Hall-effect sensors. (B-D) HD, LD, and MD kerf cells.

Slider Pad: The slider pad follows a similar end-behavioral design as the circle pad that is employed in the gaming portable Nintendo 3DS (Figure 13). In the example here, six individual kerf-unit cells are interconnected via their inter-cellular bridges. For the compound-cell, it's four corners has a an arm piece that secures the circular joystick towards the center, unattached to the compound kerf cells beneath it. The user can apply force to the circular joystick to move it across the normal of the kerf compound cell along the direction of the arms and also in combination across the other arms as well. The center-most kerf unit-cell is used as a constraint, where it's junction geometry is fixed by nails onto a support base.

Rotational Dial: The rotational dial (Figure 1 C) leverages the deformation dynamics between the constrained middle geometry of the kerf pattern and the rotational force applied across all junction beams. Varying the cut density (Low, Medium, and High) and material (PLA, TPU, and PLA-TPU bilayer composition) can influence the rotational deformation, which will be detailed in the following section for its mechanical behavior characterization. As the control ring situated on the top rotates and its deformation is resisted by the kerf pattern, the sensitivity of changes create potential haptic feedback (i.e., felt rigidity of controlling the tangible widget).

3.5.2 Global Shape and Placement Angles of Kerf Patterns.
For some 3D-printed kerf structures, using a handle for deformation may not be feasible if the structure is meant for non-stationary applications. In such cases, an alternative to a handle is needed.

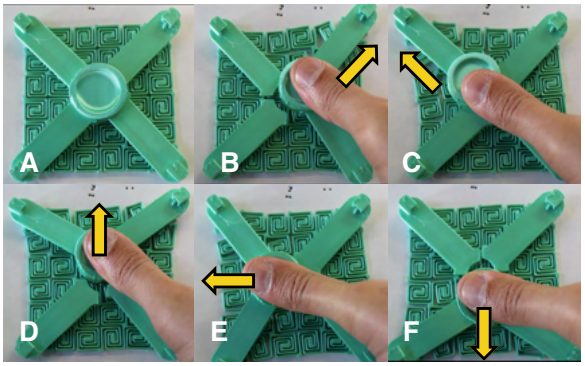

Figure 13: Slider pad in action, moving the controller towards. (A) Default state. (B-C) Upper left and right diagonal movement. (D-F) Diagonal arm directions combined for cardinal movement.

In this section, we provide two examples demonstrating how kerf structures can be deformed without conventional handles.

Robotic Gripper: Metamaterial mechanisms [19–21] refer to how metamaterials are used to creation of objects that allow for controlled directional movement, enabling the creation of objects that perform specific mechanical functions. The gripper is an example of a meta-material mechanism, extending its capability through out-of-plane deformation and its varying mechanical properties (e.g., strength, friction, etc.) to grab objects of various sizes, shapes, and textures.

The gripper design relies on out-of-plane deformations, with inter-cellular unit cells bending along the cut axis and bridge beams. A nylon fishing line through the gripper digits actuates these deformations, enabling force propagation. Thinner sections enhance curling, a specific out-of-plane deformation for the gripper.

Kerf-structured grippers offer advantages over solid-material grippers by deforming in orthogonal columns, increasing contact surfaces with objects. Unlike laser-cut joints, which are limited by material thickness and prone to waste and overheating, 3D-printed kerf structures combine material flexibility with kerf dynamics for effective bending (See Figure 17). As demonstrated in different designs with thicker kerfs (phalanx) and thinner kerfs (joints), tailored curvatures and joint arrangements enables gripping various targets with different physical traits (Figure 1 D-K, 21). Additionally, local subcell deformation enhances friction for gripping, and multi-material printing further improves surface friction. We will discuss the details in the later section.

Wearable Band: The flexibility of the kerfed sheet allows for stretching and twisting, ideal for on-body wearables. It uses in- and out-of-plane deformations to move Hall sensors and magnets embedded in TPU connectors.

Our design utilizes in- and out-of-plane deformations at the compound-cell scale. Figure 14 A (top) shows the bi-layer composition of PLA (gold) and TPU (gray) laid flat. Junction beams in each kerf unit cell are thicker, serving as posts for sensor units. The first TPU block connector holds a Hall sensor with a DuPont connector inside, the second lacks the sensor, the third contains a 2.5 mm neodymium magnet, and the fourth lacks a magnet.

Figure 14 A (bottom) shows the sensing components in detail. Figure 15 presents an exploded view of the bi-layer wearable band and its parts. In Figure 15 A, posts extrude from the junction beams of each kerf-cell, securing magnet and Hall sensor connectors to detect local deformations from user joint movements.

The wearable detects local and global movements through the sub-cells' deformation within the interconnected geometry. Magnetic field changes sense kerf-geometry deformation in both out-of-plane directions (Figure 14 B and C). It can be used for motion tracking or joint assessment, attached to the body with medical-grade tape (Figure 14 D and Figure 16).

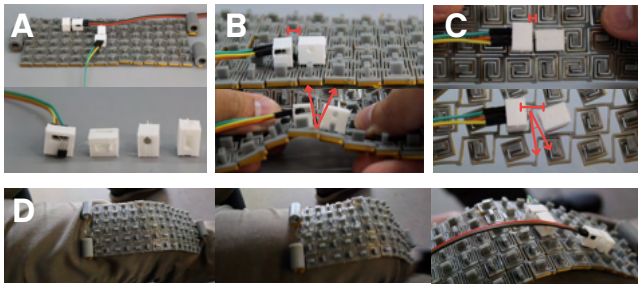

Figure 14: Kerf-structure wearable can be attached to a joint region of the body to detect movement.

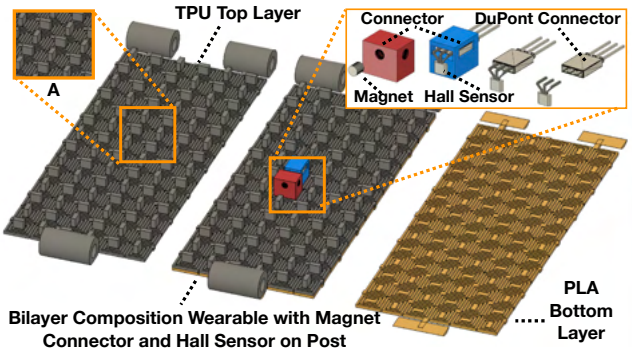

Figure 15: Explosion diagram of kerf-structure wearable. The wearable's main body consists of a top-facing TPU layer (gray) with a bottom facing PLA layer (gold).

3.5.3 Additional TPU Layers for Friction. The gripper design can be modified depending on what exactly the user intends to grab. In J and K of Figure 1 the same gripper design is modified where the number of interconnected square kerf segments are increased from three unit cells to five segments, alongside a TPU based claw attached at the end of the fingers. We use this extended gripper modification to compensate not only for size of larger objects but also their weight such as for large apples or grapefruits. Figure 17 shows a minimal version of the gripper with digits. In this version of the gripper, we reduced the total fingers from four to two, reduce connected kerf unit-cell segments to three for each finger, and we apply a thin layer of TPU (depicted as white in the top layer) to support the grip of small scale objects like cherry tomatoes.

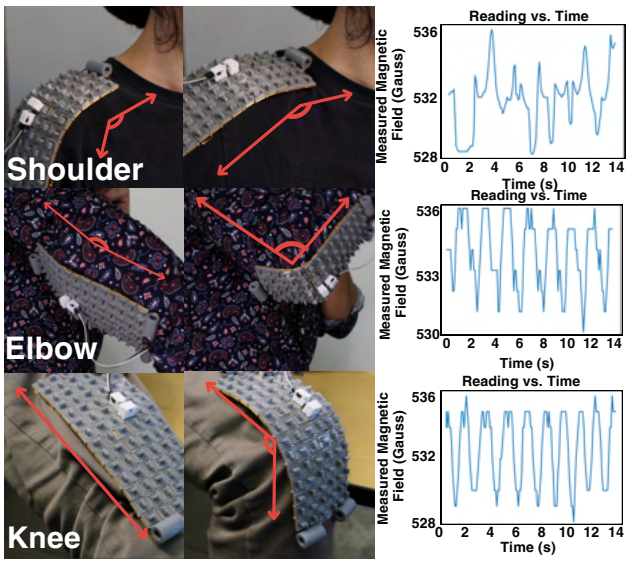

Figure 16: Kerf-structure wearable placed at different joints sense local deformations driven by repeated joint movement.

Figure 17: Minimal robotic gripper with PLA main body (green) with TPU (white) layer tip for small scale objects.

3.5.4 Justification of 3D Printed Kerf Objects in Comparison with Commercially Available Equivalent. We have identified several 3D-printed kerf interactive devices, but their practicality compared to commercial alternatives remains unclear. While ready-made electronics are easy to purchase, 3D-printed kerf objects can be customized and integrated into other designs. This flexibility allows users to modify form factors, add sensing techniques, and adapt devices to specific needs, making them more versatile for different applications.

4 Guiding Principles: Designing Interaction Using Kerf Behaviors

Due to the metamaterial nature of kerf, their parameters present unique effects in designing stand-alone, or embedded kerf-structures for interaction design. Below, we provide guidelines on how different design variables of 3D-printed kerf design can inform output deformation behavior. Designers should consider the relationship between input forces and output behaviors as this influences users' perceived sensitivity and feedback using 3D-printed kerf devices.

4.1 Common Traits of Kerf with Geometry-related Parameters

In applying kerf patterns for interactive applications, cell shape, cut density, pattern type, and alignment are universal parameters, derived directly from the 2D geometry of the kerf pattern. Below we will describe briefly how they can inform end-use.

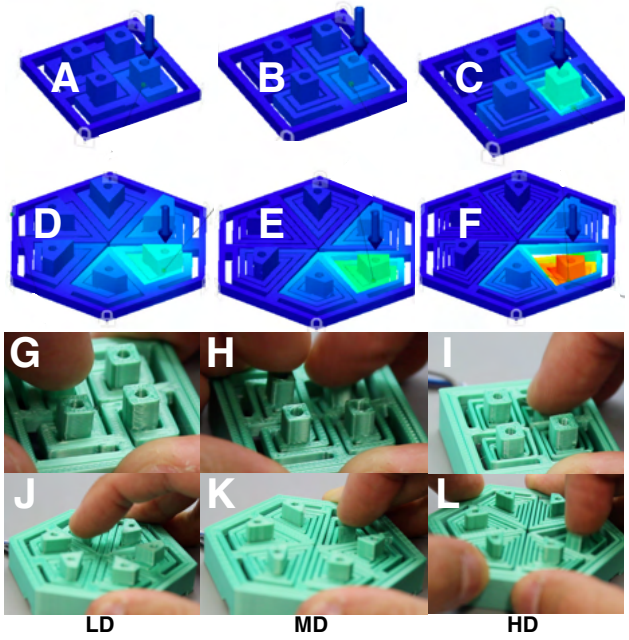

Figure 18: Density of cut concentrations varied across LD, MD, and HD types, affecting the extent to push-down deformation resistance (A–F). Push-button across kerf-cell pattern types and cut densities (G–L).

4.1.1 ***Principle #1. Increased Cut Density Adds More Degrees of Freedom under Applied Force.*** The shape of the kerf unit-cell type influences how many spiral cuts are present in its geometry which in turn influences the degree to which the cells can actuate before mechanical failure and the load that can be placed on them. In Figure 18, we illustrate the differences in deformation between square and hexagon kerf unit cells when their beam thickness is held constant. Square kerf cells are more rigid to deformation than hexagonal cells but can withstand a greater load (Figure 18). If the dimension of two unit cells are the same, shape would not necessarily control force and displacement dynamics, but rather the slenderness ratios of the beam segments in the square and hexagon cells respectively. If one were to scale the size of the hexagon unit cells so that each beam segment has about the same slenderness ratio as the one in the square, we would get about the same magnitude of deformation and force.

Increasing the density of cuts decreases the load-bearing capacity but increases the flexibility within the unit cell. This can influence how much the kerf unit cell can deform under applied force, affecting the degree of deformation relative to its density (Figure 18). The extent to which kerfing allows local flexing is subject to the density of cut lines within the pattern, influencing flexibility. Low-cut density results in low flexibility and higher load-bearing capability, whereas high-cut density results in more flexibility but lower load-bearing capability. Immediately, designers should be aware of the relationship between cut density and degree of deformation as it gives a consistent baseline for expectation for end-effects.

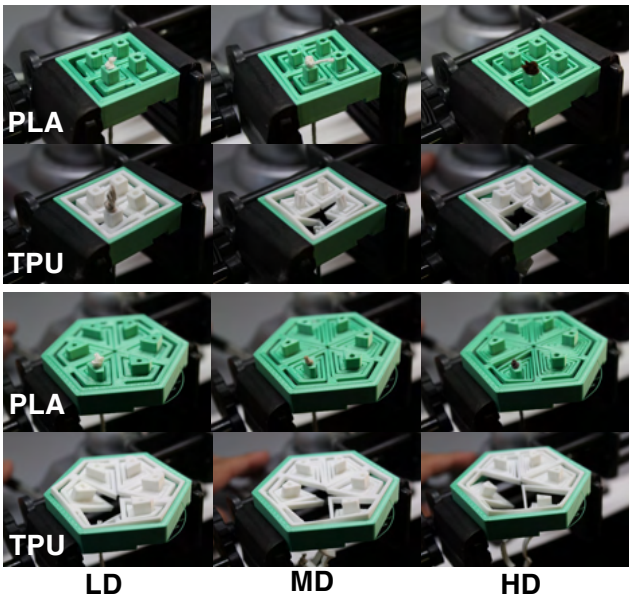

Figure 19: Kerf push button across shape (square on top and hexagon on bottom) and cut-density variations with a 150 gram weight pulling button held by a vice grip.

4.1.2 ***Principle #2. Lower Cut Density Results in Greater Passive Force Feedback by Reduced Degrees of Freedom.*** If kerf unit-cell patterns are directly used as interactive primitives in button, dial, and slider, the force applied to deform the objects also results in passive feedback, experienced in various ways such as responsiveness, smoothness, or hardness of the interaction. Figure 19 illustrates how pattern type can influence the end-user experience with kerf-based objects. This is attributed to the amount of force needed to deform the object and the resultant deformation from this force application. We use a force distance curve to compare square and hexagon kerf-unit cells through a simulation of applied force ranging from 25 grams to 150 grams (Figure 20). Comparing displacement and increasing force between high cut-density square and hexagon kerf-unit cells (HD-SQ and HD-HEX, respectively), we see that the square kerf cell has a higher gradation of displacement with increasing force, but the extent of resultant displacement is less than that of the hexagon kerf-unit cell.

Similarly, comparing across cut-density variations, we see similar trends for the respective shape types. Interestingly, the displacement and associated force remain close in gradation at the low and medium cut-density variations, but there is a sudden change in gradation when both patterns reach the high cut-density variations.

Altogether, designers can take away the following points. When holding cut-density constant between square and hexagon kerf-unit cells, the square kerf can be characterized as resistive to greater loads, whereas the hexagon kerf-cell can be characterized as more compliant with less force required to deform. For designers, this implies that the choice of kerf-unit cell type can influence how users perceive the effects of their actions using kerf-based devices.

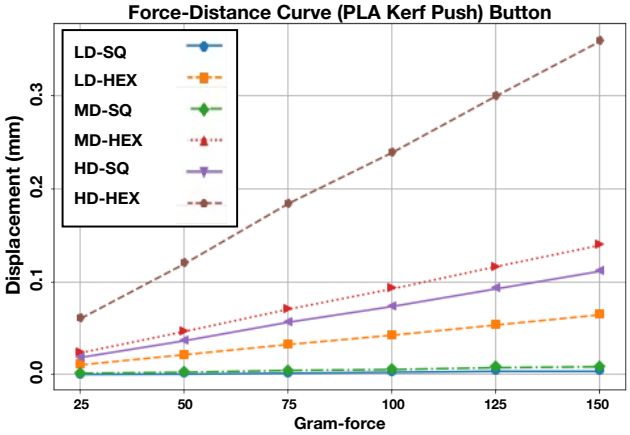

Figure 20: Force-Displacement curve illustrating differences in displacement of kerf push buttons under varying forces across variations of shape and cut-density patterns.

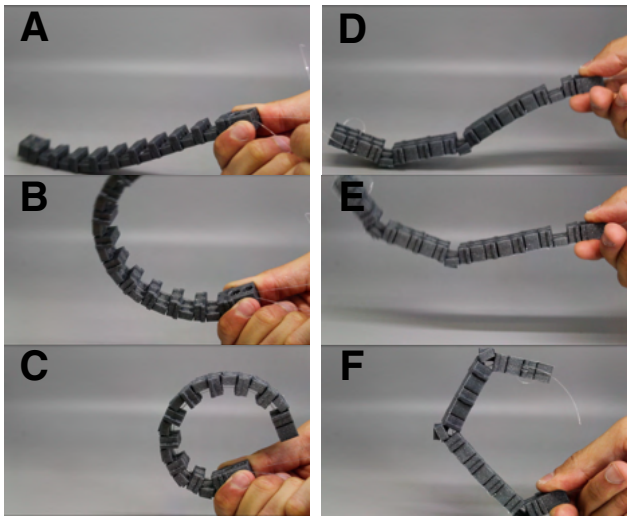

Figure 21: The gripper is modified where the thickness of the finger variably deforms under force.

4.1.3 ***Principle #3. Relative Kerf cell alignment can control the global deformation pattern.*** By linking multiple unit cells together, the more the aggregate can deform, producing a multiplicative effect in deformations as demonstrated in Figure 21. Here, there are selected sub-cells that are less thick than their neighboring groups of interconnected sub-cells (A-C). Designers can connect consecutive unit-cells together for a combined geometry that has more flexibility than its individual composing unit-cells. In the square kerf gripper, the respective square kerf unit cells are fairly stiff, yet when linked together, the macroscopic bend that is achieved increases as more of them are linked. This same macroscopic bend can be adjusted by the thickness of kerf-unit cells, resulting in a non-uniform curvature in comparison to the original gripper finger design (D-F). Such changes lead to the gripper finger taking on a more humanoid finger curvature.

By linking together multiple unit cells together, the interaction space (for in-plane and out-of-plane) increases (Figure 22). It matters for designers where depending on the scale of the interaction space, this can dictate how many unit-cells may be needed to achieve an end-function. We saw this in the case of the gripper, where the gripper was modified to grasp object at different scales, compensating for their relative shape and volume.

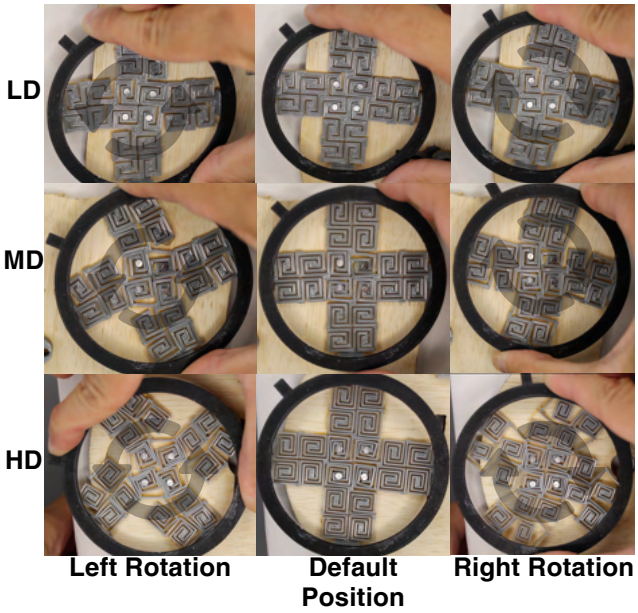

Figure 22: Square-kerf pattern gains increased rotational deformation capability by connecting co-located unit-cells.

4.1.4 ***Principle #4. The thicker beams consisting of kerf require more force to deform.*** Increasing the thickness of uncut material results in objects that require more force to deform and take on more load. The thinner the object, the more flexible the deformations are but the weaker the load. In Figure 24 we have 3 hexagon kerf patterns of the same cut density with the same force (20N) applied (Figure 24). What we can see is that same force results in reduced displacement as the kerf object becomes thicker.

Designers need to take interest in thickness as there is a fair balance to consider for the degree of flexibility coupled with the kind of force need to output or the extent the object can take on a load. This was the case for the multiple iterations of the gripper where

we experimented with different thicknesses (Figure 21), finding that more thickness supports require more force to flex while imparting a greater load as well. Regarding its kinematics, in order for the gripper to function without visible fibers outside of the kerf, there needed to be non-uniform thickness between sections to allow for a bend. This informed how to design the *"dips"* in the gripper, balancing between how much thickness was needed to support deformation while supporting an applied load.

4.2 3D Printing Exclusive Kerf Parameters

In 3D printed kerf structures, material type and thickness are exclusive parameters. This is because 3D printing determines the materials that can be used (i.e., filament type), and thickness can vary within the fabricated kerf structure, resulting in heterogeneous thickness and anisotropic characteristics due to the layer-by-layer construction method of 3D printing.

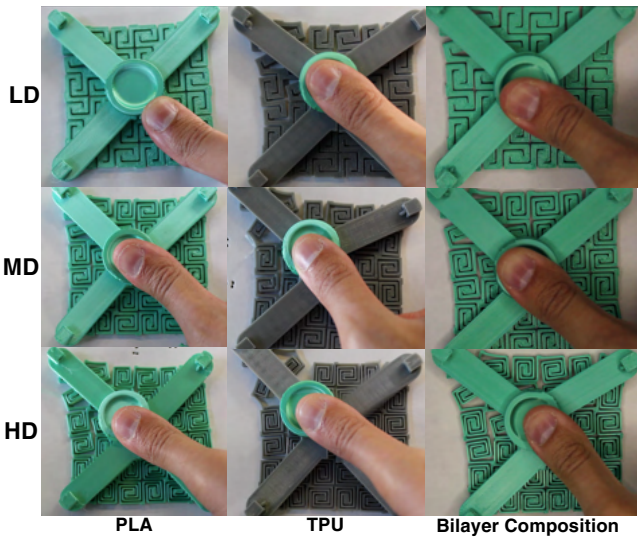

Figure 23: Material and cut-density variations of the slider with the same force applied to their respective control arms.

4.2.1 ***Principle #5. Filament Types Influence the Extent of Kerf Deformation.*** The material properties, respectively or as combined, of the filament influence the degree to which the kerf geometry can be deformed when used in a design. This has implications for how the deformation can be specifically tuned based on the composition of the filament and its layout. Figure 23 illustrates these effects in material variations of the slider application. First column presents three cut variations for the PLA slider, where only the HD variation becomes responsive to force. If we compare the same pattern variations in TPU at the second column, where the slider deforms farther and easier even at lower cut densities. However, at the HD variation, going past the catching arms of the slider. When holding kerf-geometry constant, we can see how the material affordances of common filaments like PLA and TPU can be a factor for designers on how the interactive kerf-device responds to user-applied force input or passive force-feedback.

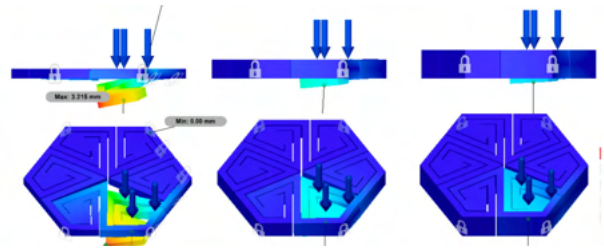

Figure 24: The kerf patterns printed in 0.125,0.25, and 0.375 inches thick, respectively. With the same force applied, thicker kerf cells deform lightly.

4.2.2 ***Principle #6. Bilayer composition can specify material affordances in user and control deformation.*** Bi-layer composition can specify and combine material affordances for both in-plane and out-of-plane deformations. In 3D-printed kerf structures, bi-layer composition indicates which regions possess specific material properties. For example, in the minimal robotic gripper shown in Figure 17, the design leverages the material properties of both PLA and TPU based on their placement in the gripper's geometry. PLA is used for the lower body of the gripper due to its stiffness and load-bearing capacity, while TPU is used in the upper sections, where it makes direct contact with gripped objects and maintains contact with TPU's surface friction.

Bi-layer composition blends the in-plane and out-of-plane deformation effects of PLA and TPU. In the slider application shown in Figure 23, we present examples using a bi-layer composition with PLA (green on top) and TPU (gray on the bottom), in the third column. Here, we demonstrate that by combining the material properties of PLA and TPU (seen in the previous columns). Each cut-density of the bi-layer design results in deformation outputs that fall between those of its PLA and TPU counterparts. For designers, the material properties of 3D-printed kerf structures affect the degree of deformation, while the arrangement of these materials in the final structure allows for fine-tuning. This involves determining the proportion of different filament materials to achieve the desired deformation and effects.

5 Validating Kerf Cell Behaviors

In the interest of understanding how 3D-printed kerf-patterns can be used for interaction, we conducted simulations and testing. These tests were performed to understand the plastic deformations of kerf unit cells and kerf aggregates to generate and retain freeform shapes as well as their response to loads. Specifically, we conducted tests across variations of unit cells fabricated from PLA, TPU, and PLA-TPU (bi-layer composition). The unit cells are based on different cut patterns and cut densities, as covered in Table 1 and Figure 10.

In terms of simulation, the kerf cells are modeled as beams, tested for bending, torsion, and stretching motions [10, 37]. We will validate kerf unit cells and their aggregations to assess their effects and feasibility in interactive applications. By examining how these two kerf cut patterns and their variations deform, we can generalize the behavior of other patterns, considering material properties and structural configurations (e.g., aggregates).

5.1 Experimental Tests and Simulations

We simulated kerf unit cells and aggregates in Abaqus/CAE, using prismatic bar segments in a finite element (FE) analysis. These simulations assessed mechanical performance under varying cut density and material composition, representing the segments as elastic isotropic materials with shell and beam elements and a solid rectangular cross-section (1-inch side lengths for hexagon and square unit cells, 0.125-inch thickness). The B31 beam element was used to analyze axial bending, twisting, and rotation, chosen for its lower computational cost.

This approach simplifies the kerf unit cell geometry, which may cause discrepancies between the simulation and experimental results, as noted by Shahid et al. and Chen et al. in their studies on laser-cut kerf cells [4, 36, 37]. These discrepancies are especially significant in low-density cut kerf cells, where the beam model yields less accurate predictions.

5.2 Results

Kerf patterns allow deformation of otherwise rigid objects when force is applied, regardless of fabrication method or material. Deformations occur both in-plane (x-y axis) and out-of-plane (x-z axis), with objects bending inward or outward under various loads, including linear and rotational forces.

The 3D printed kerf-unit cell response to forces is shown below, based on prior simulations and experimental validations [9, 10], which confirmed agreement between physical and simulated results. Three types of deformations were examined: out-of-plane bending, in-plane rotation, and out-of-plane rotation. Out-of-plane bending occurs by applying a normal force while constraining the edges. In-plane deformations involve spiral beams displacing linearly and rotationally along the applied force axes. Out-of-plane rotation is achieved by holding one edge of the cell and rotating it along an in-plane axis.

Figure 25 shows the effect of bending on the square kerf unit cell for different kerf densities and material types. Ksi (kilo-pounds per square inch) measures stress. TPU, with its lower stiffness, shows higher flexibility, while higher cut densities result in lower stresses for the same displacement.

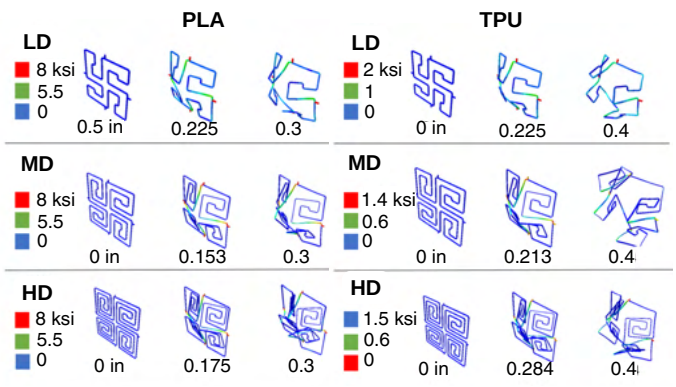

Figure 25: Out of plane bending of PLA (left) and TPU (right) for the square kerf unit cell of different densities.

Figure 26 shows the square unit cell's response to rotation for different kerf densities and material combinations. Stiffness decreases from PLA to 50:50 bi-layer to TPU, reflecting the stress patterns. PLA with low density generates the highest stresses, while TPU with high density produces the lowest. There is a trade-off between deflection capacity and rigidity. Material changes have a greater impact than density changes. Depending on the application, the material-property and unit-cell geometry interplay can guide the selection of the appropriate unit cell.

Hexagonal kerf unit cells were tested under similar conditions, focusing on PLA material to observe responses to bending, rotation, and twisting (Figure 27). Larger and geometrically distinct from square cells, hexagonal cells tolerate greater deflection without failure. This concludes the force analyses, demonstrating how kerf cells balance flexibility and rigidity, enduring various forces based on their geometry and material.

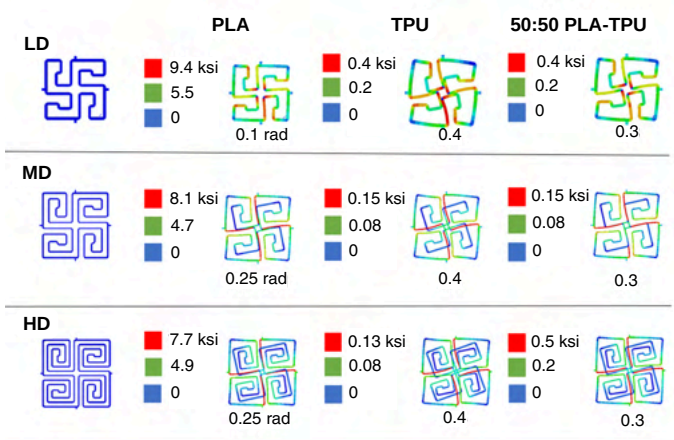

Figure 26: In plane rotation of PLA (left) and TPU (right) for the square kerf unit cell of different densities.

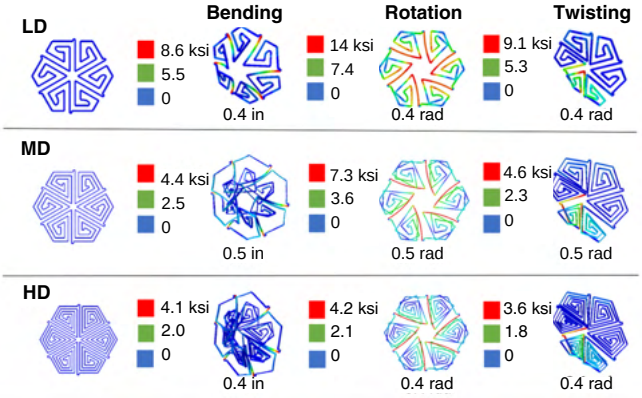

Figure 27: Hexagon Kerf cells (PLA) of different densities being subject to bending, rotation and twisting.

The material of kerf cells/aggregates can further influence flexibility with TPU kerf cells being much more flexible than PLA due to TPU's lower elastic modulus. Simulated and experimental results confirm the viability of 3D-printed kerf unit cells/aggregates in designing mechanical metamaterials (Figures 28, 29, and 30). The comparison includes gripper fingers with thicknesses of 0.0625 inches (left) and 0.0125 inches (right).

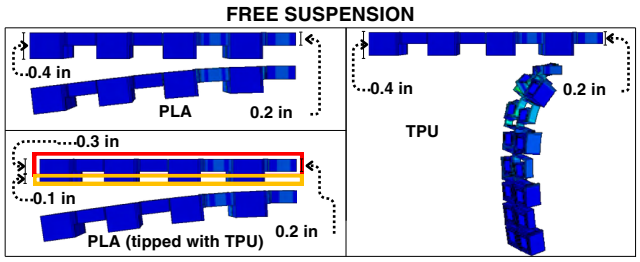

Figure 28: Influence of PLA, TPU, and PLA/TPU mix in free suspension.

From Figure 30, it can be observed that the fingers made with PLA slightly flexes across thicknesses (A and B) while TPU flails downward when freely suspended (C and D) TPU having a much higher density lower stiffness when compared with PLA are the factors influencing this behavior. It has also been demonstrated that again due these differences in material properties, more force is required to perform the same displacement actuation on PLA when compared to TPU. However, more force would mean a higher holding force and PLA being more stiffer can hold a heavier specimen without flexing. But, it has been experimentally observed that the flexible TPU has better grip due to it being deformed at the contact surface, and creating more friction. A finger made with PLA, but tipped with TPU at the points of contact would provide the advantages of both the scenarios (Figure 29 and Figure 30 (E and F)). If one desires to have less force while actuation, they can explore with varying kerf densities or use a 50:50 bi-layer composition to make the finger. An exploration of these options can be performed based on the context of use for the gripper finger, using simulations to guide the design refinements of expected outcome.

Kerf cells and their aggregates enable planar structures to deform under in-plane and out-of-plane forces, producing output forces for local and global deformation. 3D-printed polymers make these structures function as compliant mechanisms, returning to their original shape unless the force exceeds the material's yield strength.

6 Discussion

6.1 Can varying the microstructure of kerf-patterns influence sensing/haptic applications towards interactive devices?

In our work, we demonstrated how varying the density of 3D-printed kerf cuts can influence the sensing and haptic feedback of interactive devices. Regarding kerf shape (Principles #1 and #2), we found that the base shape of a kerf pattern, determined by the number of cut spirals, affects its deformation. For instance, the square kerf pattern was relatively rigid compared to the hexagon

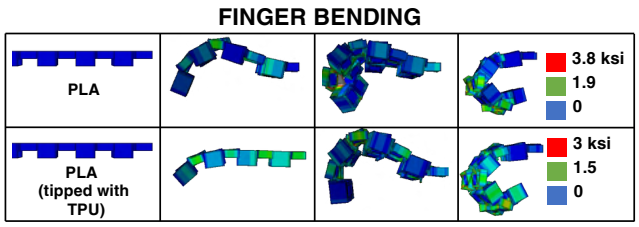

Figure 29: Influence of PLA and PLA/TPU mix in finger gripper deformation.

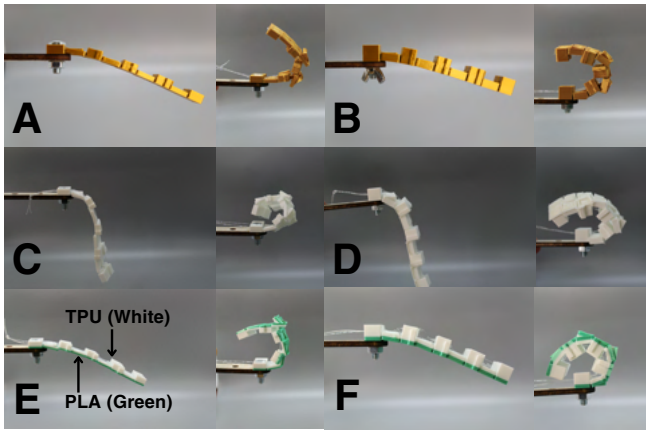

Figure 30: Validation of influence of PLA, TPU, and PLA/TPU bi-layer composition in deformation of kerf gripper finger.

pattern, which deformed more easily. This suggests that the hexagonal pattern is better suited for sensing applications. In a push-button application, at the lowest cut density, the hexagonal pattern allowed easier alignment of the embedded magnet with the hall sensor, while the square pattern required significantly more force and exhibited less deformation. Another observation concerns the passive feedback experienced by the user when applying force to a given shape pattern (Principle #4). The pattern's shape influences the extent of deformation, leading end-users to describe certain kerf patterns as 'responsive,' 'compliant,' or 'hard' depending on the force applied.

Cut density and thickness significantly impact sensing and passive feedback (Principles #2 and #4). In the push-button application, the square kerf pattern was ineffective at low cut density, but increasing it improved deformation, making it similar to the hexagon pattern. For the hexagon pattern, higher cut density enhanced deformation. Additionally, increasing thickness required more force to achieve the same displacement. These findings suggest that designers can control deformation, sensing, and feedback by adjusting shape topology, thickness, and cut density. This approach can tailor buttons for high-performance use (e.g., for gaming controllers) or everyday environments (e.g., in public elevators).

We demonstrated how 3D-printed kerf patterns leverage their deformation capabilities for both in-plane and out-of-plane applications, with interconnecting kerf cells enhancing these effects. Through several proof-of-concept examples, such as the pinball

spring, slider, and dial, we showed that kerf cells deform locally, and these deformations multiply when combined. For instance, in the slider application, arms at the four corners of a square kerf compound cell allowed us to use a central puck to move the arms and pull the connected kerf cells. In the pinball spring, a portion of a compound cell was attached to a housing with a hall sensor, and pulling a handle caused the sensor to detect magnetic field changes. Rotational deformation was achieved by fixing the central geometry and connecting kerf cell endpoints to a rotating ring, causing the kerf cells to rotate with the ring.

6.2 What are the advantages of multi-materials?

The effects of kerfing in kerf-cut patterns stem from the geometric properties of these patterns, rather than the fabrication method itself. We have shown how 3D-printed kerfed objects are created using a subtractive manufacturing technique. By applying kerf effects to 3D printing, we harness the unique properties of materials and the capabilities of the fabrication process.

Two unique advantages of 3D printing kerf structures are the material properties and their influence on deformation, sensitivity, and passive feedback (Principle #5). As observed in the slider application, different filaments impact deformation under applied force. For example, PLA required more force and resulted in less displacement, while TPU works in opposite. However, the material choice isn't always straightforward. In the kerf push-button, the TPU version is easier to press, but the PLA version provides more resistance and better compliance for returning to its default position. For designers, material selection influences how a 3D-printed kerf object performs and is perceived.

Second, the organization of materials within 3D-printed kerf structures offers added benefits for end applications (Principle #6). In our gripper example, we used a bilayer composition with TPU in the contact region and PLA in the load-bearing areas. This allowed the gripper to maintain a stronger hold while preserving its structural integrity. We also observed that the bilayer composition of PLA and TPU resulted in intermediary deformation effects, offering customized deformation outcomes based on material proportions. This suggests that designers can tailor deformation characteristics by adjusting material distribution in kerf objects.

The stiffness of a kerf structure depends not only on material but also on its geometry. While homogeneous materials lead to predictable stiffness, using multiple materials within a kerf structure alters this dynamic. Thinner regions are not necessarily more flexible than thicker ones when different materials are used. By combining materials and geometry, we enhance spatial tunability and degrees of freedom (DOF), something not achievable by varying only the kerf cut topology in a single material. For example, using only stiff PLA for flexibility would require many cuts, weakening the structure, while flexible materials like TPU could cause collapse. Combining materials with kerf patterns can overcome these limitations.

6.3 Limitations and Future Work

Our main contribution is understanding the interplay between geometry and material behavior in 3D printing through empirical design experiments. We defined the input space (what can be changed) and the output space (what can and cannot be controlled), validating this approach through simulations. While this method is not yet ready for end-user design replication, particularly without parametric tools, improving replicability and ease of use through such tools will be our next focus.

While our work provides clear design principles individually, their combined effects remain less understood. We focus on establishing discrete principles to first understand microstructure behavior before analyzing their interaction on a larger scale. Future work is needed to explore these interactions, as a comprehensive study of the numerous design parameters in kerf structures, both geometric and 3D printing-related, would require separate investigation. This approach will inform the development of a parametric modeling tool for target users. In designing the parametric toolkit, we will integrate our principles into a user-centered approach. This will require a holistic user study involving the many design parameters of kerf structures. The results will guide the development of modeling tools, offering end-users high-level abstractions of parameters and their behaviors through simulations.

We also acknowledge limitations in 3D-printed kerf structures, particularly their material properties and layer-by-layer fabrication, as discussed in section 2.3. Over time, these devices may wear out or experience permanent deformation if overextended, limiting their long-term durability. Different materials like PLA and TPU have varying strengths and weaknesses, which can affect their practical use. Future work will explore how composite materials can enhance the durability of interactive kerf structures.

7 Conclusion

Designers and engineers have long sought to combine elasticity and hardness to create objects that are both strong and flexible. Kerfing, a subtractive method traditionally used in woodworking, achieves these properties. With the increasing accessibility of additive manufacturing tools, the concept of kerfing can now be utilized by designers, engineers, and everyday users to create materials that are both durable and flexible.

While novel materials like TPU can be extruded or cast in factories, a broader range of material options is available through multi-material and composite 3D printing [9, 10]. Effective cutting of these materials would require different settings for each layer, as laser cutting assumes a homogeneous material composition. Additionally, although many materials can be laser cut, some composites cannot be processed due to their fiber arrangement. 3D printing kerfs enables a wider variety of materials to be used and combined, either as bilayers or composites [9, 12].

By additively manufacturing kerf-pattern-based objects with interconnected meandering unit-cells, we present an approach to using 3D-printed kerf structures that can be tailored to user contexts and expected end behaviors. Our design guidelines offer a mapping of kerf-unit cell behaviors under different application conditions, demonstrating how various attributes can be leveraged for end-use.

Acknowledgments

This research is partly supported by the NSF grant CMMI 2222935 and AFOSR FA 9550-23-1-0734. We also thank TAMU High Performance Computing Center for the computational support.

References

[1] Bernd Bickel, Moritz Bächer, Miguel A Otaduy, Hyunho Richard Lee, Hanspeter Pfister, Markus Gross, and Wojciech Matusik. 2023. Design and fabrication of materials with desired deformation behavior. In *Seminal Graphics Papers: Pushing the Boundaries, Volume 2*. 829–838.

[2] Ignazio Blanco. 2020. The use of composite materials in 3D printing. *Journal of Composites Science* 4, 2 (2020), 42.

[3] Sebastien JP Callens and Amir A Zadpoor. 2018. From flat sheets to curved geometries: Origami and kirigami approaches. *Materials Today* 21, 3 (2018), 241–264.

[4] Renzhe Chen, Coby Turman, Mingliang Jiang, Negar Kalantar, Michael Moreno, and Anastasia Muliana. 2020. Mechanics of kerf patterns for creating freeform structures. *Acta Mechanica* 231 (2020), 3499–3524.

[5] Renzhe Chen, Coby Turman, Mingliang Jiang, Negar Kalantar, Michael Moreno, and Anastasia Muliana. 2020. Mechanics of kerf patterns for creating freeform structures. *Acta Mechanica* 231 (2020), 3499–3524.

[6] Xiang'Anthony' Chen, Jeeeun Kim, Jennifer Mankoff, Tovi Grossman, Stelian Coros, and Scott E Hudson. 2016. Reprise: A design tool for specifying, generating, and customizing 3D printable adaptations on everyday objects. In *Proceedings of the 29th Annual Symposium on User Interface Software and Technology*. 29–39.

[7] Jungsoo Choi, Ryoonhan Kim, Danbi Song, Dae-Won Cho, Jeong Suh, Seonmin Kim, and Sang-Hyun Ahn. 2022. Analysis of laser cutting process for different diagonal material shapes. *Processes* 10, 12 (2022), 2743.

[8] Cristina-Daria Condoroţeanu, Lidia Gurău, Camelia Coşereanu, and Sergiu-Valeriu Georgescu. 2022. A proposed method to evaluate the effect of changing the kerfing parameters upon the static bending behavior of flexible plywood panels cut by laser. *Applied Sciences* 12, 9 (2022), 4303.

[9] Aryabhat Darnal, Kanak Mantri, Will Betts, Negar Kalantar, Jeeeun Kim, and Anastasia Muliana. 2024. Flexibility, Toughness, and Load Bearing of 3D-Printed Chiral Kerf Composite Structures. *Composites Part B: Engineering* (2024), 111685.

[10] Aryabhat Darnal, Kanak Mantri, Zaryab Shahid, Negar Kalantar, and Anastasia Muliana. 2023. The influence of inelastic materials on freeform kerf structures. *Thin-Walled Structures* 193 (2023), 111292.

[11] Aryabhat Darnal, Kamal Poluri, Himani Deshpande, Jeeeun Kim, Negar Kalantar, and Anastasia Muliana. 2023. An exploration of 3D printed freeform kerf structures. In *Proc. of SPIE Vol*, Vol. 12484. 124840A–1.

[12] Aryabhat Darnal, Zaryab Shahid, Himani Deshpande, Jeeeun Kim, and Anastasia Muliana. 2023. Tuning mechanical properties of 3D printed composites with PLA: TPU programmable filaments. *Composite Structures* 318 (2023), 117075.

[13] Aryabhat Darnal, Zaryab Shahid, Himani Deshpande, Jeeeun Kim, and Anastasia Muliana. 2023. Tuning mechanical properties of 3D printed composites with PLA: TPU programmable filaments. *Composite Structures* 318 (2023), 117075.

[14] Adel Gani, William Ion, and Erfu Yang. 2021. Experimental investigation of plasma cutting two separate thin steel sheets simultaneously and parameters optimisation using Taguchi approach. *Journal of Manufacturing Processes* 64 (2021), 1013–1023.

[15] Silvio Genna, Erica Menna, Gianluca Rubino, and Vincenzo Tagliaferri. 2020. Experimental investigation of industrial laser cutting: The effect of the material selection and the process parameters on the kerf quality. *Applied sciences* 10, 14 (2020), 4956.

[16] Orkan Zeynel Guzelci, Sema Alaçam, and Saadet Zeynep Bacınoğlu. 2017. Three-step experimentation on embedding curvature to rigid planar materials through cut patterns. *Gestão & Tecnologia de Projetos* 12, 3 (2017), 93–107.

[17] Juan-Juan Han and Han-Xiong Huang. 2011. Preparation and characterization of biodegradable polylactide/thermoplastic polyurethane elastomer blends. *Journal of Applied Polymer Science* 120, 6 (2011), 3217–3223.

[18] Syed Fouzan Iftekar, Abdul Aabid, Adibah Amir, and Muneer Baig. 2023. Advancements and limitations in 3D printing materials and technologies: a critical review. *Polymers* 15, 11 (2023), 2519.

[19] Alexandra Ion, Johannes Frohnhofen, Ludwig Wall, Robert Kovacs, Mirela Alistar, Jack Lindsay, Pedro Lopes, Hsiang-Ting Chen, and Patrick Baudisch. 2016. Metamaterial mechanisms. In *Proceedings of the 29th annual symposium on user interface software and technology*. 529–539.

[20] Alexandra Ion, Robert Kovacs, Oliver S Schneider, Pedro Lopes, and Patrick Baudisch. 2018. Metamaterial textures. In *Proceedings of the 2018 CHI Conference on Human Factors in Computing Systems*. 1–12.

[21] Alexandra Ion, Ludwig Wall, Robert Kovacs, and Patrick Baudisch. 2017. Digital mechanical metamaterials. In *Proceedings of the 2017 CHI Conference on Human Factors in Computing Systems*. 977–988.

[22] Vladislav Jašo, Miroslav Cvetinov, Srđan Rakić, and Zoran S Petrović. 2014. Bioplastics and elastomers from polylactic acid/thermoplastic polyurethane blends. *Journal of Applied Polymer Science* 131, 22 (2014).

[23] David Rayner Hunkin Jones and Michael F Ashby. 1993. *Engineering materials*. Elsevier.

[24] NEGAR KALANTAR and ALIREZA BORHANI. [n. d.]. INFORMING DEFORMABLE FORMWORKS. ([n. d.]).

[25] N Kalantar and A Borhani. 2018. Informing deformable formworks, parameterizing deformation behavior of a non-stretchable membrane via kerfing. In *Learning, Prototyping and Adapting—Proceedings of the 23rd CAADRIA Conference*, Vol. 2. 339–348.

[26] Barbara Ruschel Lorenzoni and Fabio Pinto da Silva. 2022. Geometric analysis of the MDF kerf-bending structure accuracy. *International Journal of Space Structures* 37, 2 (2022), 135–149.

[27] Qian Lu, Aryabhat Darnal, Haruki Takahashi, Anastasia Hanifah Muliana, and Jeeeun Kim. 2022. User-Centered Property Adjustment with Programmable Filament. In *CHI Conference on Human Factors in Computing Systems Extended Abstracts*. 1–6.

[28] Rimma Melnikova, Andrea Ehrmann, and Karin Finsterbusch. 2014. 3D printing of textile-based structures by Fused Deposition Modelling (FDM) with different polymer materials. In *IOP conference series: materials science and engineering*, Vol. 62. IOP publishing, 012018.

[29] Tolga Mert. 2012. Water jet cutting technology and its comparison with other cutting methods in some aspects. *Academic Journal of Science* 1, 3 (2012), 275–282.

[30] PRILAGOJENIH OSEBNIM POTREBAM OPORNIC. 2019. Application of a thermoplastic polyurethane/polylactic acid composite filament for 3D-printed personalized orthosis. *Materiali in tehnologije* 53, 1 (2019), 71–76.

[31] Julian Panetta, Qingnan Zhou, Luigi Malomo, Nico Pietroni, Paolo Cignoni, and Denis Zorin. 2015. Elastic textures for additive fabrication. *ACM Transactions on Graphics (TOG)* 34, 4 (2015), 1–12.

[32] Sebastian W Pattinson, Meghan E Huber, Sanha Kim, Jongwoo Lee, Sarah Grunsfeld, Ricardo Roberts, Gregory Dreifus, Christoph Meier, Lei Liu, Neville Hogan, et al. 2019. Additive manufacturing of biomechanically tailored meshes for compliant wearable and implantable devices. *Advanced Functional Materials* 29, 32 (2019), 1901815.

[33] Jayson Paulose, Anne S Meeussen, and Vincenzo Vitelli. 2015. Selective buckling via states of self-stress in topological metamaterials. *Proceedings of the National Academy of Sciences* 112, 25 (2015), 7639–7644.

[34] Edwin A Peraza-Hernandez, Darren J Hartl, Richard J Malak Jr, and Dimitris C Lagoudas. 2014. Origami-inspired active structures: a synthesis and review. *Smart Materials and Structures* 23, 9 (2014), 094001.

[35] Christian Schumacher, Bernd Bickel, Jan Rys, Steve Marschner, Chiara Daraio, and Markus Gross. 2015. Microstructures to control elasticity in 3D printing. *ACM Transactions on Graphics (Tog)* 34, 4 (2015), 1–13.

[36] Zaryab Shahid, Coleman Gustav Bond, Molly Saylor Johnson, James E Hubbard Jr, Negar Kalantar, and Anastasia Muliana. 2022. Dynamic response of flexible viscoelastic kerf structures of freeform shapes. *International Journal of Solids and Structures* 254 (2022), 111895.

[37] Zaryab Shahid, James E Hubbard, Negar Kalantar, and Anastasia Muliana. 2022. An investigation of the dynamic response of architectural kerf structures. *Acta Mechanica* (2022), 1–25.

[38] Aristidis Tsiolikas, John Kechagias, Konstantinos Salonitis, and Nikos Mastorakis. 2016. Optimization of cut surface quality during CNC Plasma Arc Cutting process. (2016).

[39] Jun Wang, Bin Yang, Xiang Lin, Lei Gao, Tao Liu, Yonglai Lu, and Runguo Wang. 2020. Research of TPU materials for 3D printing aiming at non-pneumatic tires by FDM method. *Polymers* 12, 11 (2020), 2492.

[40] Willa Yunqi Yang, Yumeng Zhuang, Luke Andre Darcy, Grace Liu, and Alexandra Ion. 2022. Reconfigurable Elastic Metamaterials. In *Proceedings of the 35th Annual ACM Symposium on User Interface Software and Technology*. 1–13.

[41] Saied Zarrinmehr, Ergun Akleman, Mahmood Ettehad, Negar Kalantar, Alireza Borhani Haghighi, and Shinjiro Sueda. 2017. An algorithmic approach to obtain generalized 2D meander-patterns. In *Proceedings of Bridges 2017: Mathematics, Art, Music, Architecture, Education, Culture*. 87–94.

[42] Saied Zarrinmehr, Mahmood Ettehad, Negar Kalantar, Alireza Borhani, Shinjiro Sueda, and Ergun Akleman. 2017. Interlocked archimedean spirals for conversion of planar rigid panels into locally flexible panels with stiffness control. *Computers & Graphics* 66 (2017), 93–102.

Received 1 August 2024; revised 14 November 2024; accepted 22 November 2024